

Diffuse supernova neutrinos: oscillation effects, stellar cooling and progenitor mass dependence

Cecilia Lunardini^{a,b} and Irene Tamborra^c

^aArizona State University, Tempe, AZ, 85287-1504, USA

^bRIKEN BNL Research Center, Brookhaven National Laboratory, Upton, NY 11973, USA

^cMax-Planck-Institut für Physik (Werner-Heisenberg-Institut)
Föhringer Ring 6, 80805 München, Germany

E-mail: Cecilia.Lunardini@asu.edu, tamborra@mpp.mpg.de

Abstract. We estimate the diffuse supernova neutrino background (DSNB) using the recent progenitor-dependent, long-term supernova simulations from the Basel group and including neutrino oscillations at several post-bounce times. Assuming multi-angle matter suppression of collective effects during the accretion phase, we find that oscillation effects are dominated by the matter-driven MSW resonances, while neutrino-neutrino collective effects contribute at the 5–10% level. The impact of the neutrino mass hierarchy, of the time-dependent neutrino spectra and of the diverse progenitor star population is 10% or less, small compared to the uncertainty of at least 25% of the normalization of the supernova rate. Therefore, assuming that the sign of the neutrino mass hierarchy will be determined within the next decade, the future detection of the DSNB will deliver approximate information on the MSW-oscillated neutrino spectra. With a reliable model for neutrino emission, its detection will be a powerful instrument to provide complementary information on the star formation rate and for learning about stellar physics.

Contents

1	Introduction	1
2	Input physics	2
2.1	Diffuse SN neutrino flux	2
2.2	Cosmological supernova rate	3
2.3	Reference neutrino signals from supernovae of different masses	4
2.4	Neutrino mixing parameters and quantum kinetic equations	5
3	Time-integrated neutrino fluxes and oscillation effects	7
4	Diffuse supernova neutrino background	10
5	Conclusions	13

1 Introduction

The Diffuse Supernova Neutrino Background (DSNB) is the flux of neutrinos and antineutrinos emitted by all core-collapse supernovae (SN) in our universe. Isotropic and stationary, it is a guaranteed signal that will give us a unique image of the SN population of the universe and of its history all the way to redshift ~ 1 or so. This image can be a precious alternative, or a unique complement, to a high statistics detection of an individual nearby SN which is a rare event (~ 1 -3 SNe per century in our galaxy [1–4]). Although the DSNB has not been detected yet, its discovery prospects are excellent. Gadolinium enriched Super-Kamiokande is expected to detect the DSNB at a level of few events per year [5, 6] and tens to hundreds of events are predicted for the next generation of larger scale, 0.1–1 Mt mass detectors, running for a few years [7, 8].

The DSNB depends on the cosmological SN rate, the neutrino fluxes and the oscillation physics. Its prediction is a challenging problem because of the still sparse astrophysical observations of supernovae, the incomplete picture of neutrino oscillation physics, and several obstacles — of theoretical and computational nature — in the way of fully modeling the neutrino emission from core collapse. Due to these difficulties, a number of simplifying assumptions were adopted to model the DSNB, typically the same neutrino spectra were used for different post-bounce times and for all progenitors and only approximate neutrino oscillation physics was considered (see [9, 10] for reviews on the topic). Only recently efforts were developed to include more accurate astrophysical information and oscillations driven by neutrino-neutrino forward scattering [11–14].

From the perspective of neutrino oscillation physics, lately new advances have taken place on the experimental and theoretical front. The elusive mixing angle θ_{13} has been measured [15, 16], leaving us only with open questions on the neutrino mass hierarchy and the CP-violating phase (although the latter does not affect neutrino oscillations in supernovae [17]). Concerning neutrino oscillations in supernovae from the theoretical perspective, the matter enhanced flavor conversion picture [18, 19] has been completed by including neutrino-neutrino interactions, responsible for the non-linear neutrino flavor evolution (see [20] for a review on the topic). The present sketch is that, during the accretion phase,

total (or partial) multi-angle matter suppression of collective oscillations is expected [21–26]; while, during the cooling phase, multiple spectral splits occur [27, 28] and Mikheev-Smirnov-Wolfenstein (MSW) resonances are expected at larger radii [18, 19]. Moreover, most recent numerical simulations of core-collapse SN provide information about neutrino spectra up to ~ 10 s post-bounce [29, 30] and for different progenitor masses [30]. Therefore the time is mature to include these updates in the estimate of the DSNB and to assess the impact of each in comparison with the many uncertainties, experimental and theoretical, that affect the diffuse flux itself. This is the goal of this paper. We model the DSNB, as consistently as possible, in the framework of the Basel model [30]. We consider oscillation physics for different post-bounce times for both neutrino mass hierarchies, including the multi-angle treatment of ν - ν interactions.

This work is organized as follows. In Section 2 we discuss the cosmological supernova rate, the adopted supernova models for different progenitor masses and we give a brief overview on neutrino oscillation physics in supernovae. In Section 3 we discuss the impact of neutrino oscillations on the neutrino time-integrated flux for a fixed supernova mass. In Section 4, we present our results on the DSNB. Conclusions and perspectives are illustrated in Section 5.

2 Input physics

In this Section, the cosmological SN rate and the reference neutrino signal for different SN masses are discussed. We also introduce the neutrino mass-mixing parameters and the quantum kinetic equations describing the neutrino oscillations in supernovae.

2.1 Diffuse SN neutrino flux

Simply put, the DSNB offers us an image of the entire SN population of the universe. It reflects the demographics of this population: how it is distributed in space, its history, the diverse sub-types that contribute to it with their different neutrino emissions. Besides, the image we get is influenced by the neutrinos’ own history, as they travel cosmic distances before they reach us. Therefore the diffuse flux of a given neutrino flavor depends on many physical quantities of different origin.

- The flux produced by an individual SN, which depends on the dynamics of the core collapse and is different for different masses of the progenitor star.
- Propagation effects: namely flavor oscillations, which depend on the neutrino masses and mixings, and the redshift of energy; for a neutrino produced at redshift z with energy E' , the observed energy is $E = E'/(1+z)$.
- The comoving SN rate (SNR), $\dot{\rho}_{\text{SN}}(z, M)$, per unit of redshift and per unit of progenitor mass M . It is defined in the mass interval between $M_0 \simeq 8 M_{\odot}$ (the minimum necessary to have a core-collapse supernova) and a maximum $M_{\text{max}} \sim 125 M_{\odot}$, the tentative upper limit for the occurrence of normal core-collapse supernovae (as opposed to pair instability ones or black-hole forming events) [11]. In terms of redshift, the SNR is largest between $z = 0$ and $z_{\text{max}} \simeq 5$, reflecting the period of most intense star formation activity (see Sec. 2.2). Note that we neglect the contribution due to failed supernovae [31].

With these ingredients, the diffuse flux for each flavor ν_β ($\beta = e, \bar{e}, \mu$ or τ) can be written as [11]:

$$\Phi_{\nu_\beta}(E) = \frac{c}{H_0} \int_{M_0}^{M_{\max}} dM \int_0^{z_{\max}} dz \frac{\dot{\rho}_{SN}(z, M) F_{\nu_\beta}(E', M)}{\sqrt{\Omega_M(1+z)^3 + \Omega_\Lambda}}, \quad (2.1)$$

where c is the speed of light and $H_0 = 70 \text{ km s}^{-1} \text{ Mpc}^{-1}$ the Hubble constant; $\Omega_M = 0.3$ and $\Omega_\Lambda = 0.7$ are the fractions of the cosmic energy density in matter and dark energy respectively and $F_{\nu_\beta}(E', M)$ is the oscillated ν_β flux for a SN with progenitor mass M (see Sec. 3). As we will see, the DSNB is dominated by the contribution of the closest ($z \lesssim 1$) and least massive ($M \sim M_0$) stars, and depends only weakly on M_{\max} and z_{\max} .

Although the DSNB has not been observed yet, interesting upper limits exist. The most stringent is on the $\bar{\nu}_e$ component of the flux, from a search of inverse beta-decay events at Super-Kamiokande, above 17.3 MeV threshold: $\phi_{\bar{\nu}_e} \lesssim 2.8\text{--}3.0 \text{ cm}^{-2}\text{s}^{-1}$ at 90% C.L. [32, 33]. This bound is generally consistent with predictions, excluding scenarios where multiple parameters conspire to generate a particularly large flux [34]. Because the search at Super-Kamiokande is background-dominated, any substantial improvement on it will require better background subtraction. Methods involving water with Gadolinium addition [5], liquid Argon [35–37], and liquid scintillator [38] are especially promising. Of these, detectors of Megaton class will have the further advantage of high statistics, yielding up to hundreds of events a year from the DSNB (see e.g., [7, 8]).

2.2 Cosmological supernova rate

Considering that SN progenitors are very short lived, the SNR is proportional to the Star Formation Rate (SFR), $\dot{\rho}_\star$, defined as the mass that forms stars per unit time per unit volume. The relationship between the SNR and SFR is given by the Initial Mass Function (IMF), $\eta(M) \propto M^{-2.35}$ [39], which describes the mass distribution of stars at birth:

$$\dot{\rho}_{SN}(z, M) = \frac{\eta(M)}{\int_{0.5M_\odot}^{M_{\max}} dM M \eta(M)} \dot{\rho}_\star(z). \quad (2.2)$$

Recent analyses of SNR and SFR measurements [40] show that a piecewise parametrization of $\dot{\rho}_\star$ is adequate [41]:

$$\dot{\rho}_\star \propto \begin{cases} (1+z)^\delta & z < 1 \\ (1+z)^\alpha & 1 < z < 4.5 \\ (1+z)^\gamma & 4.5 < z \end{cases}. \quad (2.3)$$

Here we adopt this function, with δ, α, γ and the normalization fixed at the best fit values [41]: $\delta = 3.28, \alpha = -0.26, \gamma = -7.8$ and $\int_{M_0}^{M_{\max}} dM \dot{\rho}_{SN}(0, M) = 1.5 \times 10^{-4} \text{ Mpc}^{-3}\text{yr}^{-1}$ (integrated SNR at the present epoch). Note that, due to the redshift of energy, neutrinos of higher redshift accumulate at lower energies, so that in the energy window relevant for experiments ($11 \text{ MeV} \lesssim E \lesssim 40 \text{ MeV}$ [6, 32]) the diffuse flux is dominated by the low z contribution, $z \lesssim 1$. Therefore, its dependence on α and γ is weak. The flux is also dominated by the lower mass stars, considering the fast decline of the IMF with M , so that there is a strong dependence on M_0 , but a weak one on the high cutoff M_{\max} .

Let us now comment on the existing measurements of the SNR and their uncertainties, which are dominated by normalization errors [3, 40]. Perhaps the most precise way to measure the SNR is from data on the SFR, via Eq. (2.2). The cosmic star formation history as a

function of the redshift is known from data in the ultraviolet and far-infrared [41]. Constraints are stronger at $z \lesssim 1$, while observations at higher redshift have larger errors. Following Ref. [40], we adopt the statistical error of about 25% as uncertainty on the normalization. This underestimates the total error, that includes a number of systematic effects, some of which are difficult to estimate.

In principle, to rely on the SFR data is not necessary: the SNR is given by direct SN observations. However, data from SN surveys are sparse (low statistics) and extend only to $z \sim 1$. The most precise measurement is the recent LOSS result for the local ($z = 0$) rate, integrated over all masses [42]: $\int_{M_0}^{M_{\max}} dM \dot{\rho}_{SN}(0, M) = (0.70 \pm 0.15) \times 10^{-4} \text{ Mpc}^{-3}\text{yr}^{-1}$. Here we use its error (dominated by systematics), of $\sim 22\%$ as a very optimistic estimate of uncertainty. Other errors are due to possible dust obscuration and supernova impostors (see [40] for details).

Surprisingly, the normalization from direct SN observations is lower than that from SFR data, by a factor ~ 2 (with a $\sim 2\sigma$ level significance at $z = 0$) and by a smaller factor at higher z [3]. A possible explanation to this mismatch is that many supernovae are missed because they are either optically dim (low-luminosity) or dark, whether intrinsically or due to obscuration. Other proposed explanations are an incomplete understanding of the star formation and supernova rates including that supernovae form differently in small galaxies than in normal galaxies [3].

Finally, a complementary constraint on the SNR normalization comes from the Super-Kamiokande limit on the DSNB (Sec. 2.1). The constraint depends on the neutrino spectrum and is strong for rather hot neutrino spectra [43]. For the cooler spectra favored by SN 1987A, data allow a normalization up to ~ 2 times higher than the value we use here.

2.3 Reference neutrino signals from supernovae of different masses

We adopt supernova simulations consistently developed over 7 s or more for three different masses ($8.8 M_{\odot}$, $10.8 M_{\odot}$ and $18 M_{\odot}$) [30]. Such core-collapse models are based on spherically symmetric general relativistic hydrodynamics and they include spectral three-flavor Boltzmann neutrino transport with the equation of state from Shen et al. [44]. However, they do not include nucleon recoil. As observed in [45], the inclusion of nucleon recoil is responsible for reducing the differences among the mean energies of different flavors during the cooling phase (otherwise different up to 10%) [29, 45, 46]. Since one of our purposes is to evaluate the impact of neutrino oscillations on the DSNB, the Basel model favors the appearance of any signature due to neutrino oscillations in the DSNB.

At a radius r , the unoscillated spectral number fluxes for flavor ν_{β} and for each post-bounce time t_{pb} are

$$f_{\nu_{\beta}}^0(E, t_{\text{pb}}) = \frac{L_{\nu_{\beta}}(t_{\text{pb}})}{4\pi r^2} \frac{\varphi_{\nu_{\beta}}(E, t_{\text{pb}})}{\langle E_{\nu_{\beta}}(t_{\text{pb}}) \rangle} = \frac{F_{\nu_{\beta}}^0(E, t_{\text{pb}})}{4\pi r^2}, \quad (2.4)$$

where $L_{\nu_{\beta}}(t_{\text{pb}})$ is the luminosity for flavor ν_{β} , $\langle E_{\nu_{\beta}}(t_{\text{pb}}) \rangle$ the mean energy, and $\varphi_{\nu_{\beta}}(E, t_{\text{pb}})$ a quasi-thermal spectrum. We describe it schematically in the form [47]

$$\varphi_{\nu_{\beta}}(E, t_{\text{pb}}) = \xi_{\beta}(t_{\text{pb}}) \left(\frac{E}{\langle E_{\nu_{\beta}}(t_{\text{pb}}) \rangle} \right)^{\alpha_{\beta}(t_{\text{pb}})} e^{-(\alpha_{\beta}(t_{\text{pb}})+1)E/\langle E_{\nu_{\beta}}(t_{\text{pb}}) \rangle}. \quad (2.5)$$

The parameter $\alpha_{\beta}(t_{\text{pb}})$ is defined by $\langle E_{\nu_{\beta}}(t_{\text{pb}})^2 \rangle / \langle E_{\nu_{\beta}}(t_{\text{pb}}) \rangle^2 = (2 + \alpha_{\beta}(t_{\text{pb}})) / (1 + \alpha_{\beta}(t_{\text{pb}}))$ and $\xi_{\beta}(t_{\text{pb}})$ is a normalization factor such that $\int dE \varphi_{\nu_{\beta}}(E, t_{\text{pb}}) = 1$.

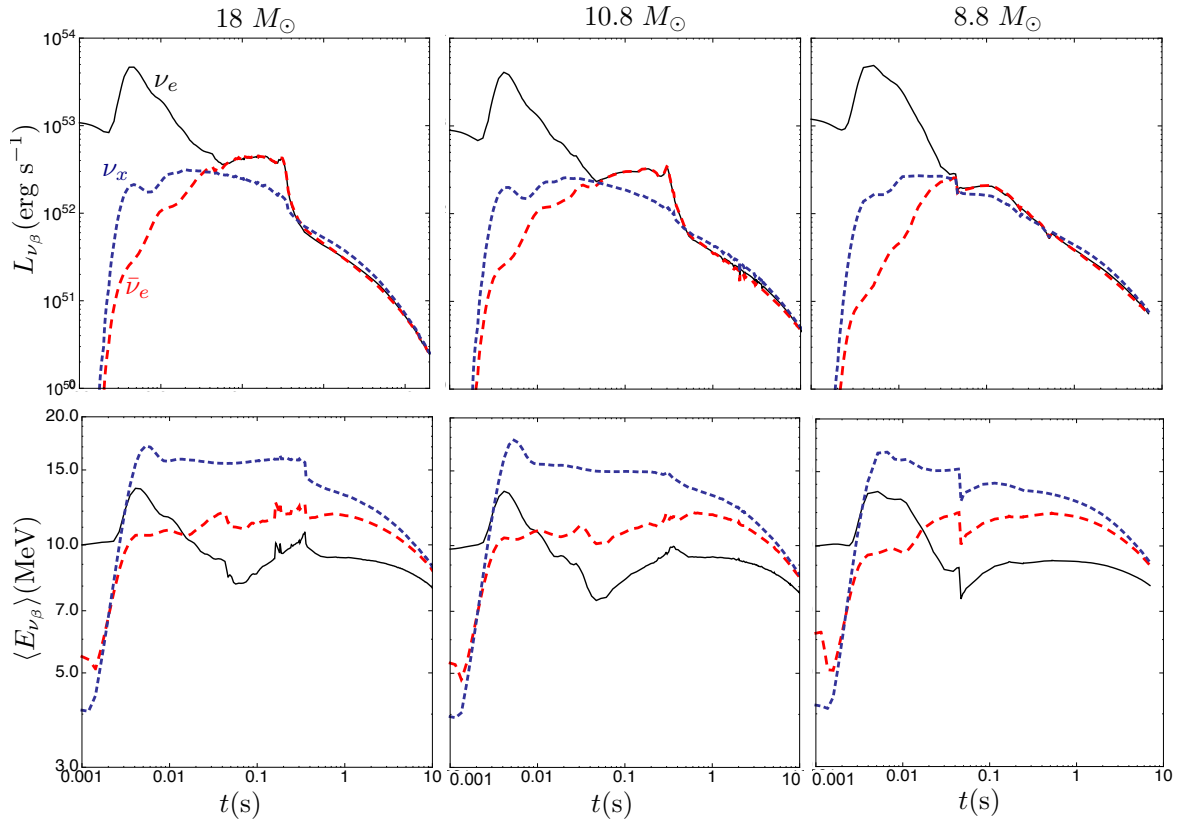


Figure 1. Luminosities (on the top) and mean energies (on the bottom) in the observer frame for three progenitors with masses $M = 18, 10.8, 8.8 M_\odot$ (from left to right) as a function of the post-bounce time [30, 48]. In blue (red, black respectively) are plotted the quantities related to $\nu_{\mu,\tau}$ and $\bar{\nu}_{\mu,\tau}$ denoted by ν_x ($\bar{\nu}_e, \nu_e$).

Figure 1 shows the luminosities (on the top) and the mean energies (on the bottom) in the observer frame for the three adopted progenitor models as a function of the post-bounce time as in [30, 48]. Note that the luminosities of the different flavors are almost equal during the accretion phase, while $L_{\nu_e} \gg L_{\bar{\nu}_e}, L_{\nu_{\mu,\tau}}$ during the cooling phase. While, the mean energies are $\langle E_{\nu_{\mu,\tau}} \rangle > \langle E_{\bar{\nu}_e} \rangle > \langle E_{\nu_e} \rangle$ during the cooling phase.

2.4 Neutrino mixing parameters and quantum kinetic equations

We assume the following neutrino mass squared differences [49]

$$\delta m_{\text{atm}}^2 = 2.35 \times 10^{-3} \text{ eV}^2, \quad (2.6)$$

$$\delta m_{\text{sol}}^2 = 7.58 \times 10^{-5} \text{ eV}^2, \quad (2.7)$$

and we discuss both normal (NH, $\delta m_{\text{atm}}^2 > 0$) and inverted hierarchy (IH, $\delta m_{\text{atm}}^2 < 0$) scenarios. The mixing angles are [49, 50]

$$\sin^2 \theta_{13} = 0.02 \text{ and } \sin^2 \theta_{12} = 0.3; \quad (2.8)$$

we neglect the third mixing angle θ_{23} for reasons that will be clear in a while.

We treat neutrino oscillations in terms of the matrices of neutrino densities for each neutrino mode with energy E , ρ_E , where diagonal elements are neutrino densities, off-diagonal

elements encode phase information due to flavor oscillations. The radial flavor variation of the quasi-stationary neutrino flux is given by the ‘‘Schrödinger equation’’

$$i\partial_r \rho_E = [\mathbf{H}_E, \rho_E] \quad \text{and} \quad i\partial_r \bar{\rho}_E = [\bar{\mathbf{H}}_E, \bar{\rho}_E], \quad (2.9)$$

where an overbar refers to antineutrinos and sans-serif letters denote 3×3 matrices in flavor space consisting of ν_e , ν_μ and ν_τ . The initial conditions are $\rho_E = \text{diag}(n_{\nu_e}, n_{\nu_\mu}, n_{\nu_\tau})$ and $\bar{\rho}_E = \text{diag}(n_{\bar{\nu}_e}, n_{\bar{\nu}_\mu}, n_{\bar{\nu}_\tau})$ where $n_{\nu_\mu} = n_{\nu_\tau} = n_{\nu_x}$ and the same for antineutrinos. The Hamiltonian matrix contains vacuum, matter, and neutrino–neutrino terms

$$\mathbf{H}_E = \mathbf{H}_E^{\text{vac}} + \mathbf{H}_E^{\text{m}} + \mathbf{H}_E^{\nu\nu}. \quad (2.10)$$

In the flavor basis, the vacuum term is a function of the mixing angles and the mass-squared differences

$$\mathbf{H}_E^{\text{vac}} = \mathbf{U} \text{diag} \left(-\frac{\omega_L}{2}, +\frac{\omega_L}{2}, \omega_H \right) \mathbf{U}^\dagger, \quad (2.11)$$

where \mathbf{U} is the unitary mixing matrix, function of the mixing angles, transforming between the mass and the interaction basis, $\omega_L = \delta m_{\text{sol}}^2/2E$ and $\omega_H = \delta m_{\text{atm}}^2/2E$. The matter term includes charged-current (CC) interactions and it is responsible for MSW resonances. In the flavor basis, it is

$$\mathbf{H}^{\text{m}} = \sqrt{2}G_F \text{diag}(N_e, 0, 0), \quad (2.12)$$

where N_e is the net electron number density (electrons minus positrons).

The corresponding 3×3 matrix caused by neutrino–neutrino interactions [51] including the multi-angle dependence is

$$\mathbf{H}_E^{\nu\nu} = \int dE' (\rho_{E'} - \bar{\rho}_{E'}) (1 - \cos \theta_{EE'}), \quad (2.13)$$

where $\theta_{EE'}$ is the angle between the momenta of the colliding neutrinos [52].

Ignoring radiative corrections, ν_μ and ν_τ are exactly equivalent in supernovae, allowing us to define an interaction basis $(\nu_e, \nu_x, \nu_y) = R^T(\theta_{23})(\nu_e, \nu_\mu, \nu_\tau)$, with $R^T(\theta_{23})$ the transpose of the rotation matrix $R(\theta_{23})$, such that effectively $\theta_{23} = 0$ [53]. Note that, in this rotated basis, the $e - y$ oscillations are driven by δm_{atm}^2 while the $e - x$ oscillations are driven by δm_{sol}^2 .

It is possible to factorize the effects of self-induced flavor conversions and the MSW resonances in most of the cases since they are occurring in well separated regions. We consider multi-angle ν – ν interactions driven by the atmospheric mass difference δm_{atm} and by the mixing angle θ_{13} between ν_e and ν_y , while the other flavor (ν_x) does not evolve. In fact the effects on collective flavor conversions induced by the third flavor are mainly of the nature of a subtle correction [20, 54–56] negligible for our purposes. The only way ν_x could affect the final neutrino spectra is by MSW transitions, occurring at larger radii than the ones where collective effects happen. Thus the fluxes after the collective oscillations ($F_{\nu\beta}^c$) are given by

$$F_{\nu_e}^c = P_c F_{\nu_e}^0 + (1 - P_c) F_{\nu_y}^0 \quad \text{and} \quad F_{\bar{\nu}_e}^c = \bar{P}_c F_{\bar{\nu}_e}^0 + (1 - \bar{P}_c) F_{\bar{\nu}_y}^0, \quad (2.14)$$

where P_c and \bar{P}_c are the ν_e and $\bar{\nu}_e$ survival probabilities after the multi-angle self-induced flavor conversions. They are functions of the neutrino energy, and depend on the mass hierarchy. The oscillated ν_y and $\bar{\nu}_y$ fluxes, $F_{\nu_y}^c$ and $F_{\bar{\nu}_y}^c$, can be estimated from the conservation of the total number of ν (and $\bar{\nu}$):

$$F_{\nu_y}^c + F_{\nu_e}^c = F_{\nu_e}^0 + F_{\nu_y}^0 \quad \text{and} \quad F_{\bar{\nu}_y}^c + F_{\bar{\nu}_e}^c = F_{\bar{\nu}_e}^0 + F_{\bar{\nu}_y}^0. \quad (2.15)$$

The third state, ν_x ($\bar{\nu}_x$), is not affected by the collective evolution, therefore $F_{\nu_x}^c(\bar{\nu}_x) = F_{\nu_x}^0(\bar{\nu}_x)$.

As we consider the self-induced neutrino oscillations as factorized from the MSW in first approximation, the fluxes $F_{\nu_\beta}^c$ will undergo the traditional MSW conversions after ν - ν interactions. In NH, the MSW resonance due to δm_{atm}^2 affects the ν_e flux while the $\bar{\nu}_e$ flux remains almost unaffected. On the other hand for IH, the same resonance affects the $\bar{\nu}_e$ flux and not the ν_e flux. The fluxes (F_{ν_e} and $F_{\bar{\nu}_e}$) reaching the earth after both the collective and MSW oscillations for NH and IH and for large θ_{13} are [13, 53, 57]:

$$F_{\nu_e}^{\text{NH}} = \sin^2 \theta_{12} [1 - P_c(F_{\nu_e}^c, F_{\bar{\nu}_e}^c, E)] (F_{\nu_e}^0 - F_{\nu_y}^0) + F_{\nu_y}^0, \quad (2.16)$$

$$F_{\bar{\nu}_e}^{\text{NH}} = \cos^2 \theta_{12} \bar{P}_c(F_{\nu_e}^c, F_{\bar{\nu}_e}^c, E) (F_{\bar{\nu}_e}^0 - F_{\nu_y}^0) + F_{\nu_y}^0, \quad (2.17)$$

$$F_{\nu_e}^{\text{IH}} = \sin^2 \theta_{12} P_c(F_{\nu_e}^c, F_{\bar{\nu}_e}^c, E) (F_{\nu_e}^0 - F_{\nu_y}^0) + F_{\nu_y}^0, \quad (2.18)$$

$$F_{\bar{\nu}_e}^{\text{IH}} = \cos^2 \theta_{12} [1 - \bar{P}_c(F_{\nu_e}^c, F_{\bar{\nu}_e}^c, E)] (F_{\bar{\nu}_e}^0 - F_{\nu_y}^0) + F_{\nu_y}^0. \quad (2.19)$$

Here we have used the fact that, by combining Eqs. (2.14, 2.15) with $\int dE (F_{\nu_e}^0 - F_{\bar{\nu}_e}^0) = \text{const.}$, one can express P_c and \bar{P}_c , for each energy, as functions of the fluxes after collective oscillations: $P_c(F_{\nu_e}^c, F_{\bar{\nu}_e}^c, E)$ and $\bar{P}_c(F_{\nu_e}^c, F_{\bar{\nu}_e}^c, E)$. These probabilities exhibit a well known step-like behavior, that appears in the fluxes F_{ν_e} and $F_{\bar{\nu}_e}$ as the so called ‘‘spectral splits’’ [28, 58]. In reality, a number of effects smooth out the splits in the observed neutrino fluxes; we discuss this point further below.

3 Time-integrated neutrino fluxes and oscillation effects

As a first step towards the calculation of the DSNB, we compute the oscillated fluxes, Eqs. (2.16)-(2.19), for each progenitor model, at fixed time snapshots (as an approximation of the continuous time evolution, which is too demanding for state of the art computers). The results are then used to obtain the ν_β and $\bar{\nu}_\beta$ fluxes integrated over the duration of the neutrino burst. For illustration, in this section we discuss the results for the $10.8 M_\odot$ progenitor; in Sec. 4 the fluxes for all progenitors will be summed up to obtain the DSNB, via Eq. (2.1).

While the MSW effect is well described analytically, the collective effects require a numerical calculation to obtain the probabilities P_c and \bar{P}_c . Let us discuss them here in more detail.

The spectral split patterns (affecting P_c and \bar{P}_c) are known to be crucially dependent on the initial relative flux densities and on the mass hierarchy. For definiteness, it is convenient to distinguish between the probabilities in the accretion phase ($t_{\text{pb}} \leq 1$ s), and those in the cooling phase ($t_{\text{pb}} \gtrsim 1$ s). In the accretion phase, the multi-angle effects associated with dense ordinary matter suppress collective effects [23–26]. Therefore, we adopt the results presented in [23, 24] for the two-flavor system (ν_e, ν_y), considering partial or no flavor conversion for several t_{pb} as in [23, 24].

During the cooling phase, the fluxes of different flavors are slightly different, and spectral splits occur for neutrinos and/or antineutrinos according to the mass hierarchy and to the number of crossings in the non-oscillated spectra (i.e., energies where $F_{\nu_e}^0(E) = F_{\nu_x}^0(E)$ and the same for $\bar{\nu}$) [27]. We calculate these effects by numerically solving Eqs. (2.9) for $t_{\text{pb}} = 1, 3, 6, 9$ s, for the system (ν_e, ν_y). Concerning the neutrino emission geometry, we assume a spherically symmetric source emitting neutrinos and antineutrinos like a blackbody surface, from a neutrinosphere with radius, R_ν , that varies with t_{pb} . We define the neutrinosphere radius as the radius where the neutrino radiation field is half-isotropic [24, 60] and we adopt

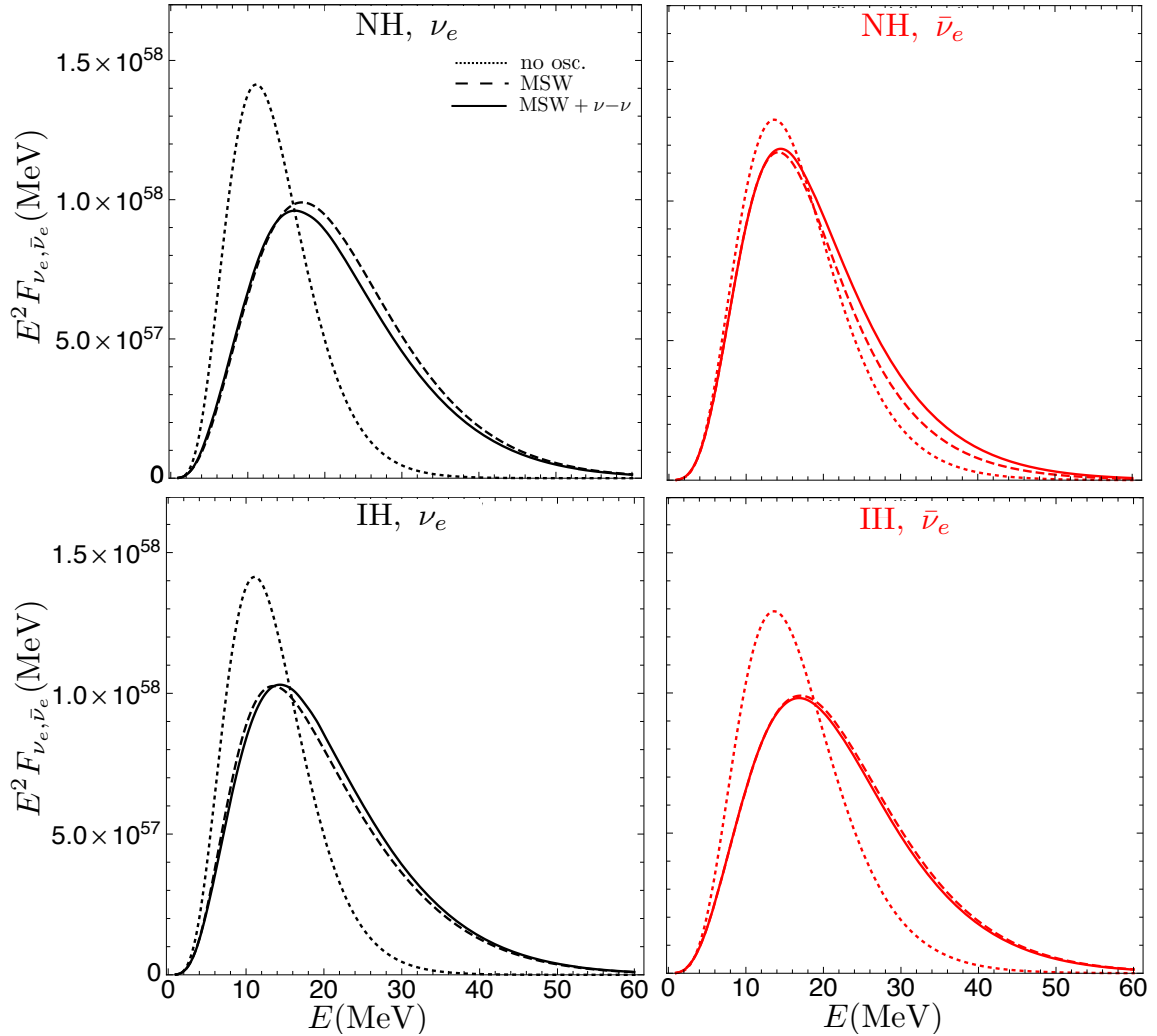


Figure 2. Time-integrated $E^2 \times F_{\nu_\beta}(E)$ fluxes as a function of the energy for $M = 10.8 M_\odot$, for ν_e ($\bar{\nu}_e$) on the left (right) and NH (IH) on the top(bottom). The non-oscillated fluxes are plotted with dotted lines, the fluxes obtained including neutrino interactions with matter only (MSW) are plotted with dashed lines and the fluxes obtained including both matter and ν background (MSW+ ν - ν) are plotted with solid lines.

the same R_ν for different flavors. Specifically, we use δm_{atm}^2 as in Eq. (2.6), $R_\nu \simeq 13$ km (although slightly varying with t_{pb}) and, to be coherent with the treatment in [23, 24], we simulate the matter effect on collective oscillations using a small, effective, in-medium mixing angle $\theta_{13,\text{eff}} = 10^{-3}$ [61]. The non-oscillated spectra are defined as in Eq. (2.5) with mean energies and luminosities as in Fig. 1.

We find that that multiple crossings appear in the non-oscillated spectra and therefore multiple spectral splits are expected during the cooling phase due to collective effects. However, the shape of the splits is smeared and their size is reduced due to the similarity of the unoscillated flavor spectra and to multi-angle effects. Often, only partial conversion is realized. In particular, for NH we find that P_c exhibits a transition from high ($P_c \gtrsim 0.6$) to low ($P_c \lesssim 0.3$) values as the energy increases, with transition energy increasing with time

from ~ 15 to ~ 35 MeV. A similar behavior is observed for \bar{P}_c for energies of relevance for detection, $E \gtrsim 5 - 7$ MeV. For IH, P_c has a somewhat opposite energy dependence, changing from $P_c \sim 0.1 - 0.3$ at $E \lesssim 15 - 20$ MeV to $P_c \gtrsim 0.6$ at higher energy. The transition becomes gentler in energy as time increases. For antineutrinos, we have $\bar{P}_c \gtrsim 0.7$ at all times and all energies, with only a moderate energy dependence. Our results for P_c, \bar{P}_c are qualitatively similar to what shown in previous literature, although smoothed by the multi-angle dependence and depending on the adopted supernova progenitor; therefore we choose to be brief here, and refer to dedicated papers for details [28, 62].

To obtain the time-integrated neutrino fluxes, we approximate the time dependence of P_c and \bar{P}_c with a step-like form, taking them to be constant in time intervals centered on the scanned t_{pb} (we adopt a time window of ~ 3 s centered on each t_{pb}). We checked that the particular choice of the time-binning affects the final results only weakly. The time-integrated fluxes have been obtained by integrating over time the fluxes computed at each time slice.

Figure 2 shows the time-integrated fluxes, $E^2 \times F_{\nu_\beta}(E)$, as a function of the energy for ν_e ($\bar{\nu}_e$) on the left (right), for both mass hierarchies for the $10.8 M_\odot$ supernova model. We distinguish among non-oscillated integrated fluxes (dotted lines), oscillated fluxes including MSW effects only (dashed lines) and oscillated fluxes including both MSW and ν - ν interactions (solid lines). Note that the MSW effect is large and generates hotter fluxes. Compared to MSW only, the collective effects produce a slight hardening or softening of the fluxes depending on the hierarchy, according to Eqs. (2.16–2.19). No signature of multiple spectral splits appear in the time-integrated flux, because they are suppressed during the accretion and they occur at different energies for each t_{pb} during the cooling; moreover multi-angle effects smear the conversion probabilities.

Overall, the flux variation due to collective effects – relative to MSW conversion only – is at the level of 10% or less. Such a small difference is explained by the fact that, in contrast with earlier approximate results on collective effects, the probabilities P_c and \bar{P}_c rarely approach zero, but remain in the interval $\sim 0.3 - 0.8$ in most cases. One should also consider that the contribution of P_c and \bar{P}_c appears in Eqs. (2.16–2.19) weighed by factors of $\sin^2 \theta_{12}$ or $\cos^2 \theta_{12}$, that reduce its size. A further reduction takes place in the time-integrated flux, which receives about 1/2 of its luminosity from the accretion phase, where collective effects are suppressed. Finally, the differences between the non-oscillated fluxes in the different flavors become progressively smaller in the cooling phase, thus suppressing any spectral change due to oscillations.

To further illustrate the size of each effect we included, in Tab. 1 we provide the mean energies and the mean squared energies for the time-integrated spectra. In the existing literature, one progenitor has been often considered as representative of the whole stellar population and one post-bounce time was taken as representative of both accretion and cooling phase. Therefore, for sake of completeness, we give this case (case a in the Table) using the parameters for $t_{\text{pb}} = 0.5$ s as representative of all post-bounce times and the $10.8 M_\odot$ progenitor as representative of the whole stellar population. Looking at the average energies in the Table, we see an expected decrease (5-10% or so) when the full cooling over ~ 10 s is included (case b), and a marked hardening due to including the MSW conversion (up to 30%, case c). As expected from Fig. 2, adding collective effects amounts to a change of 10% or less (case d), and only a very minor hardening is due to summing the results for different progenitor masses (case e). In the next Section, we will discuss in detail the differences among the different cases for the DSNB.

	a	b	c	d	e
$\langle E_{\nu_e} \rangle_{\text{NH}}$ (MeV)	9.53	8.96	12.24	11.90	11.96
$\langle E_{\nu_e}^2 \rangle_{\text{NH}}$ (MeV ²)	113.85	100.18	209.53	198.13	199.66
$\langle E_{\bar{\nu}_e} \rangle_{\text{NH}}$ (MeV)	11.82	10.84	11.23	11.50	11.62
$\langle E_{\bar{\nu}_e}^2 \rangle_{\text{NH}}$ (MeV ²)	174.20	149.17	165.88	176.72	179.62
$\langle E_{\nu_e} \rangle_{\text{IH}}$ (MeV)	9.53	8.96	10.83	11.08	11.23
$\langle E_{\nu_e}^2 \rangle_{\text{IH}}$ (MeV ²)	113.85	100.18	162.56	170.62	174.48
$\langle E_{\bar{\nu}_e} \rangle_{\text{IH}}$ (MeV)	11.82	10.83	12.24	12.17	12.18
$\langle E_{\bar{\nu}_e}^2 \rangle_{\text{IH}}$ (MeV ²)	174.20	149.17	209.53	206.77	206.06

Table 1. Mean energies and mean squared energies for the the time-integrated $F_{\nu_\beta}(E)$. The different cases considered are: (a) $F_{\nu_\beta}(E)$ obtained considering $t_{\text{pb}} = 0.5$ s as representative of all post-bounce times and the $10.8 M_\odot$ progenitor as representative of the whole stellar population, no oscillations; (b) $F_{\nu_\beta}(E)$ obtained considering time-dependent fluxes for the $10.8 M_\odot$ model, no flavor oscillations; (c) $F_{\nu_\beta}(E)$ obtained considering time-dependent fluxes for the $10.8 M_\odot$ model, MSW flavor conversions; (d) $F_{\nu_\beta}(E)$ obtained considering time-dependent fluxes for the $10.8 M_\odot$ model, MSW + ν - ν interactions; (e) $F_{\nu_\beta}(E)$ obtained including the whole stellar population, time-dependent fluxes, MSW + ν - ν interactions.

4 Diffuse supernova neutrino background

After computing the time-integrated spectra for each of the considered SN progenitors as explained in Sec. 3, we derive the DSNB, Φ_{ν_β} , using Eq. (2.1). We adopt the $8.8 M_\odot$ SN as representative of supernovae with mass in the interval $[8, 10] M_\odot$, the $10.8 M_\odot$ SN for masses in the interval $[10, 15] M_\odot$ and the $18 M_\odot$ progenitor for $M > 15 M_\odot$. Note that the for the first interval we adopt the widest range expected for O-Ne-Mg core formation.

Figure 3 shows the DSNB, $E^2 \times \Phi_{\nu_\beta}$ with Φ_{ν_β} , as a function of the energy for ν_e ($\bar{\nu}_e$) on the top (bottom). In the plots on the right, we focus on the region of interest for Super-Kamiokande detection ($E > 17.3$ MeV) and it is possible to appreciate a maximum variation of 10–20% (at $E \simeq 20$ MeV) related to the mass hierarchy. In order to favor a comparison with the existing literature, we show the fluxes obtained by taking the $10.8 M_\odot$ progenitor as representative of all progenitors (thin curves), and the full result that includes the variation of the fluxes and probabilities with the progenitor mass (thick lines). Due to the similarity of the initial luminosities and mean energies (see Sec. 3) the differences between the two cases are of few per cent.

Shock effects in Fe-core supernovae manifest themselves during the cooling phase and at large radii. We choose to neglect such effects for the $18 M_\odot$ and $10.8 M_\odot$ models because they practically might affect the δm_{atm}^2 -driven resonance only for the late cooling phase having a negligible impact on the DSNB. On the other hand, the $8.8 M_\odot$ model has a Ne-O-Mg core and the first hundreds of milliseconds of the burst are affected by variations of the matter density profile due to the shock passage. The shock wave is responsible for turning the flavor conversions from non-adiabatic to adiabatic within the first ~ 250 ms affecting the δm_{atm}^2 -driven resonance [63]. However, a very small time-window would have been affected by the shock passage in the electron-capture SN and we expect its impact on the total DSNB to be negligible.

Recently, it has been observed that the non-forward neutrino scattering contribution might affect flavor conversions during the accretion phase [64, 65]. These studies reveal that the consequences of non-forward scatterings are negligible for large SN masses when com-

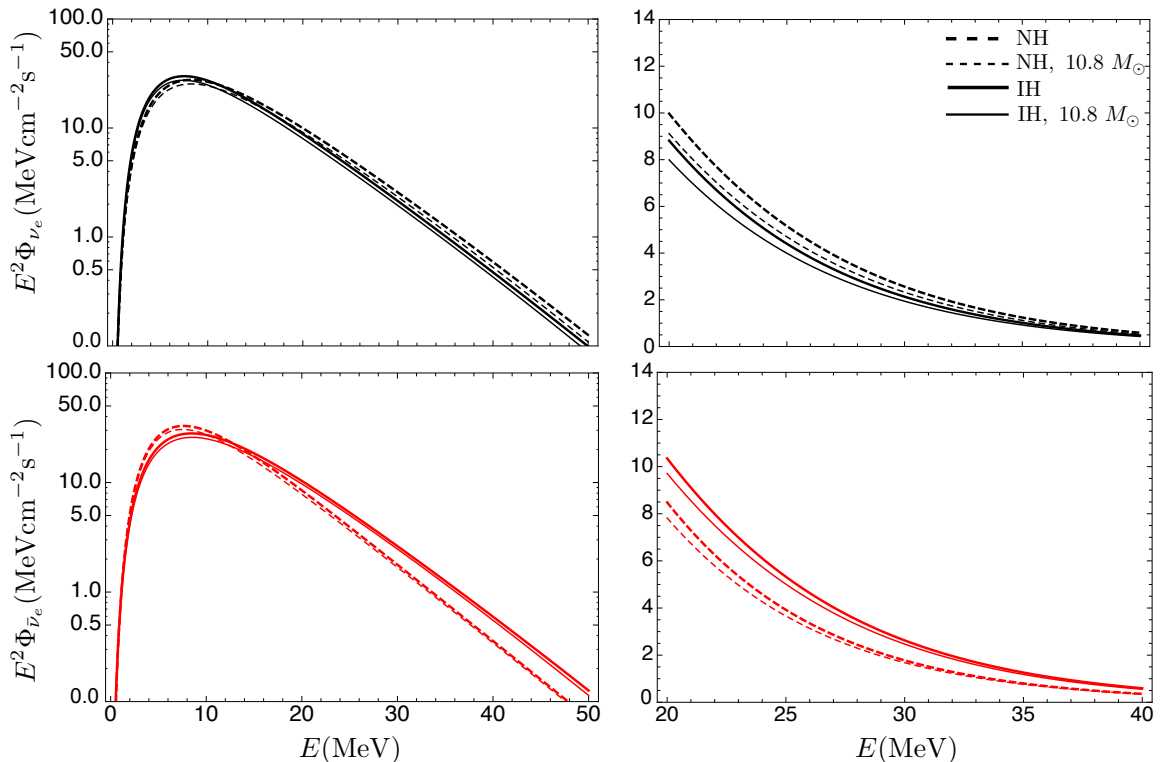


Figure 3. DSNB as a function of the energy ($E^2 \times \Phi_{\nu_e, \bar{\nu}_e}$) on the left panels, zoom in the region of Super-Kamiokande detection in the right panels ($E > 17.3$ MeV). The ν_e ($\bar{\nu}_e$) flux is plotted in black (red). The solid (dashed) line represents the DSNB in IH (NH). To mark the effects induced by the inclusion of different SN model, the thick lines represent the DSNB including the three different SN progenitors and the thin line is the DSNB obtained extending $10.8 M_\odot$ to the whole stellar population.

plete matter suppression occurs [65] and for low mass supernovae as the Ne-O-Mg ones [64]. However, it might be still relevant for supernovae with intermediate masses (as the $10.8 M_\odot$ model). Since these studies are still embryonal and no numerical implementation of the non-forward contribution is available yet, a priori, one could expect larger flavor conversions induced by the non-forward term during the accretion phase especially for the intermediate SN mass range. Therefore, we chose to adopt a parametric study of the accretion phase for the $10.8 M_\odot$ model, considering two extreme cases of full flavor conversions ($P_c = 0$) and complete matter suppression ($P_c = 1$) due to multi-angle matter effects, other than the intermediate scenario presented in [23–25]. We find that, at the level of the DSNB, after summing the fluxes from progenitor of different masses, the difference between the two cases (not shown here) is of the order of few per cent.

Figure 4 gives results for the DSNB integrated in energy above the experimental threshold 17.3 MeV [32]. It shows results for the cases (a-e) of Tab. 1 for both mass hierarchies. The differences between these cases reflect the results found for an individual SN burst in Sec. 3, with more emphasis on the high energy part of the neutrino spectrum (due to our high integration threshold). Compared to static spectra (case a), the effect of the time-dependence of the spectra over the 10 s of the neutrino burst is responsible for a variation of 6% (case b). The MSW effects (case c) are the largest source of variation of the DSNB with respect to the case without oscillations and it is about 50–60%. This variation is particularly evident for

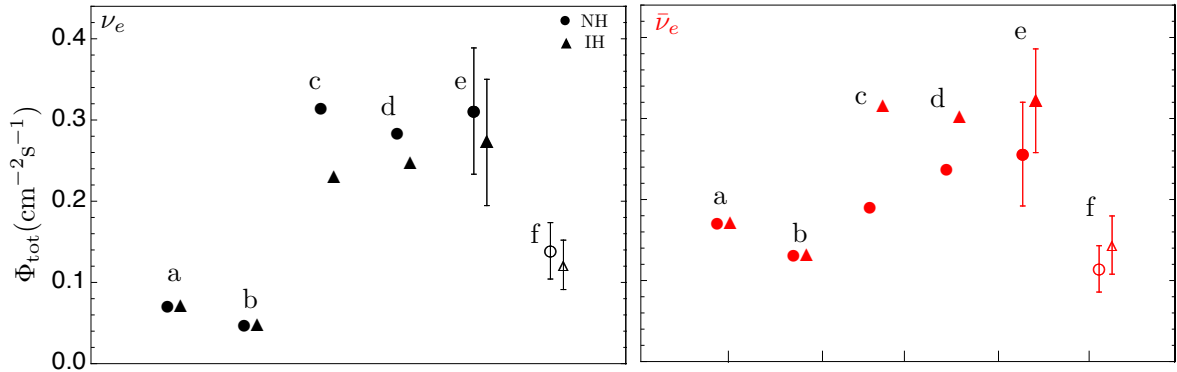


Figure 4. Energy integrated DSNB (for $E > 17.3$ MeV) as a function of the discussed contributions, in black (red) for ν_e ($\bar{\nu}_e$). We adopt triangles (dots) for the IH (NH) scenario. From left to right the source of variation of the DSNB are: (a) DSNB for $t_{\text{pb}} = 0.5$ s as representative of all post-bounce times and the $10.8 M_{\odot}$ progenitor as representative of the whole stellar population, no oscillations; (b) DSNB obtained considering time-dependent fluxes for the $10.8 M_{\odot}$ model, no flavor oscillations; (c) DSNB obtained considering time-dependent fluxes for the $10.8 M_{\odot}$ model, MSW flavor conversions; (d) DSNB obtained considering time-dependent fluxes for the $10.8 M_{\odot}$ model, MSW + ν - ν interactions; (e,f) DSNB obtained including the whole stellar population, time-dependent fluxes, MSW + ν - ν interactions; the difference in the two points is due to the factor of ~ 2 between the results of SN surveys and those of star formation measurements (see Sec. 2.2). The error bars are the errors on the normalization of the supernova rate [3].

neutrinos and the NH, where the difference between the unoscillated and oscillated spectra is the largest, due to the complete flavor permutation driven by the large θ_{13} . Neutrino-neutrino interactions (case d) are responsible for a variation of 5–10% with respect to the MSW only case. Summing over the stellar population (case e) is responsible for a DSNB variation of 5–10% due to the more luminous fluxes of the more massive stars. For sake of completeness, we provide the numerical values for the DSNB for the case (e):

$$\begin{aligned} \Phi_{\text{tot}}^{\nu_e, \text{NH}} &= 0.31 \text{ cm}^{-2} \text{ s}^{-1} \text{ and } \Phi_{\text{tot}}^{\nu_e, \text{IH}} = 0.27 \text{ cm}^{-2} \text{ s}^{-1} , \\ \Phi_{\text{tot}}^{\bar{\nu}_e, \text{NH}} &= 0.26 \text{ cm}^{-2} \text{ s}^{-1} \text{ and } \Phi_{\text{tot}}^{\bar{\nu}_e, \text{IH}} = 0.32 \text{ cm}^{-2} \text{ s}^{-1} . \end{aligned} \quad (4.1)$$

The maximum impact given by the mass hierarchy is 20%, triangle and dot in (e). It is realized for antineutrinos because, for large θ_{13} , the high density MSW resonance is adiabatic and the $\bar{\nu}_e$ flux changes from almost complete survival for NH (survival probability ~ 0.7 – 0.8) to almost complete conversion for IH (survival probability ~ 0.1 – 0.2). We estimate the DSNB taking into account the unexplained factor of ~ 2 between the results of SN surveys and those of star formation measurements as discussed in Sec. 2.2, points (e) and (f). This mismatch is responsible for the largest astrophysical source of error on the estimation of the DSNB, $\sim 50\%$. Moreover, the error on the normalization of the supernova rate is about 25% and it is represented by the error bars in (e) and (f). However, this error could be most likely higher once several systematic errors are included.

Another potential source of error on the DSNB is in the equation of state of nuclear matter used in core collapse simulation (assumed fixed in all our computations). The variation of the total neutrino energy release during the supernova explosion reflects the variation of the gravitational binding energy of the neutron star in dependence of different nuclear equations of state (see [66] for details). However, we expect that the differences of the time-integrated

emitted neutrino spectra using different equations of state will be not large enough to play a role in comparison with the other astrophysical uncertainties discussed in this paper.

5 Conclusions

The diffuse supernova neutrino background is an integrated picture of all the core collapse supernovae of different progenitor mass and redshift, and has realistic chances to be detected in the near future by upcoming experiments. The predictions for this flux have been constantly updated to include new understanding of SN physics and astrophysics, and of neutrino phenomenology. We present one such update, to include, as consistently as possible, the results of new supernova simulations and oscillation calculations.

Specifically, our calculation is the first that uses neutrino fluxes that are numerically calculated over the entire ~ 10 s of the neutrino emission for a set of different progenitor masses. For each progenitor star, we study neutrino oscillations at different times post bounce, for both the neutrino mass hierarchies, including multi-angle collective effects and adopting the recently measured value of θ_{13} . The results are then used to obtain the time-integrated flux from a single SN; finally, the oscillated fluxes for different progenitor masses are combined together into a prediction for the DSNB.

The results of this paper rely on the Basel simulation of neutrino emission [30]. Although model dependent, they are indicative of what might be expected from state of the art simulations. In particular, the Basel model has the largest spectral differences between the neutrino flavors, and therefore it is useful to estimate the largest oscillation effects that can be realistically expected.

Let us summarize our main results.

- The inclusion of time-dependent neutrino spectra are responsible for a colder neutrino spectrum compared to calculations using a fixed spectrum from early time emission (e.g., $t_{\text{pb}} \sim 0.5$ s). For a single supernova, the effect is a $\sim 5\%$ shift in the average energies (Tab. 1), which translates into a $\sim 5\%$ difference in the integrated DSNB above a 17.3 MeV threshold (Fig. 4).
- The largest effect of flavor oscillations is due to the matter-driven MSW resonances ($\sim 50\text{--}60\%$), while neutrino-neutrino collective effects give a further $\sim 5\text{--}10\%$ contribution. Moreover, the DSNB does not present any energy-dependent signature of the collective oscillations. For fixed SN progenitor, multi-angle matter effects suppress collective oscillations in the accretion phase, while multiple spectral splits occur in the cooling phase. However, such splits occur at different energies for different post-bounce times and are smeared by multi-angle effects, disappearing in the DSNB by the integration over the time and over the SN population.
- The dependence on the mass hierarchy is of the order $10 - 20\%$ (Figs. 3 and 4) and it is strongest for antineutrinos. This is because, with the recently measured large value of θ_{13} , the high density MSW resonance is adiabatic and $\bar{\nu}_e$ change from almost complete survival (survival probability $\sim 0.7 - 0.8$) to almost complete conversion (survival probability $\sim 0.1 - 0.2$) as the mass hierarchy changes from normal to inverted.
- Combining results for different progenitor stars, instead of using the $10.8 M_{\odot}$ spectra for all stars, tends to increase the DSNB by $\sim 5 - 10\%$, due to the more luminous fluxes of the more massive stars.

In summary, we find that, in first approximation, the DSNB can be described by a simplified model with a fixed, time independent spectrum for all supernovae, with MSW oscillations. The error due to neglecting the other effects that we have studied here is of the order of ten per cent or less and, assuming that the sign of the mass hierarchy will be known within the next decade and the picture of neutrino oscillations in supernovae will not drastically change in the next future, such error will be only related to the modeling of neutrino emission. We note that this error is smaller than astrophysical uncertainties: the error on the normalization of the supernova rate alone is at least 25%, and most likely higher once several systematic errors are included (among these, the still mysterious factor of ~ 2 between the results of SN surveys and those of star formation measurements). In addition to these, one should also consider errors at neutrino detectors, especially those due to the high level of background.

In consideration of errors and experimental challenges, how likely is it that the effects we have discussed will have any relevance in future data analyses? When the DSNB will be detected, probably a first phase of data analysis will focus on excluding a number of models of neutrino spectra and SNR. In this respect, to model the DSNB as accurately as possible will be important to correctly establish or exclude compatibility. To actually test for effects at the 10% level will require long term progress to reduce at least some of the uncertainties of experimental and theoretical nature. For example, with new, precise measurements of the SNR and of the sign of the neutrino mass hierarchy from beams, and reliable neutrino spectra from future simulations (or from a galactic SN), it might be possible to use the DSNB to tests the luminosity of the neutrino fluxes from lesser known SN with high mass progenitors.

Acknowledgments

We are grateful to Tobias Fisher for providing the supernova data and for useful discussions. We also thank Georg Raffelt for valuable discussions concerning this work and comments on the manuscript. This work was partly supported by the Deutsche Forschungsgemeinschaft under grant EXC-153, by the European Union FP7 ITN INVISIBLES (Marie Curie Actions, PITN-GA-2011-289442) and by the NSF grant PHY-0854827. I.T. acknowledges support from the Alexander von Humboldt Foundation and thanks Arizona State University for hospitality during the final stages of this work.

References

- [1] N. Arnaud, M. Barsuglia, M. -A. Bizouard, V. Brisson, F. Cavalier, M. Davier, P. Hello and S. Kreckelbergh *et al.*, “Detection of a close supernova gravitational wave burst in a network of interferometers, neutrino and optical detectors,” *Astropart. Phys.* **21**, 201 (2004) [gr-qc/0307101].
- [2] S. 'i. Ando, J. F. Beacom and H. Yuksel, “Detection of neutrinos from supernovae in nearby galaxies,” *Phys. Rev. Lett.* **95**, 171101 (2005) [astro-ph/0503321].
- [3] S. Horiuchi, J. F. Beacom, C. S. Kochanek, J. L. Prieto, K. Z. Stanek and T. A. Thompson, “The Cosmic Core-collapse Supernova Rate does not match the Massive-Star Formation Rate,” *Astrophys. J.* **738** (2011) 154 [arXiv:1102.1977 [astro-ph.CO]].
- [4] M. T. Botticella, S. J. Smartt, R. C. Kennicutt, Jr., E. Cappellaro, M. Sereno and J. C. Lee, “A comparison between star formation rate diagnostics and rate of core collapse supernovae within 11 Mpc,” arXiv:1111.1692 [astro-ph.CO].

- [5] J. F. Beacom and M. R. Vagins, “Antineutrino spectroscopy with large water Čerenkov detectors,” *Phys. Rev. Lett.* **93** (2004) 171101 [hep-ph/0309300].
- [6] S. Horiuchi, J. F. Beacom and E. Dwek, “The Diffuse Supernova Neutrino Background is detectable in Super-Kamiokande,” *Phys. Rev. D* **79** (2009) 083013 [arXiv:0812.3157 [astro-ph]].
- [7] A. de Bellefon *et al.*, “MEMPHYS: A Large scale water Čerenkov detector at Frejus,” hep-ex/0607026.
- [8] K. Nakamura, “Hyper-Kamiokande: A next generation water Čerenkov detector,” *Int. J. Mod. Phys. A* **18** (2003) 4053.
- [9] J. F. Beacom, “The Diffuse Supernova Neutrino Background,” *Ann. Rev. Nucl. Part. Sci.* **60** (2010) 439 [arXiv:1004.3311 [astro-ph.HE]].
- [10] C. Lunardini, “Diffuse supernova neutrinos at underground laboratories,” arXiv:1007.3252 [astro-ph.CO].
- [11] S. i. Ando and K. Sato, “Relic neutrino background from cosmological supernovae,” *New J. Phys.* **6** (2004) 170 [astro-ph/0410061].
- [12] S. Galais, J. Kneller, C. Volpe and J. Gava, “Shockwaves in Supernovae: New Implications on the Diffuse Supernova Neutrino Background,” *Phys. Rev. D* **81** (2010) 053002 [arXiv:0906.5294 [hep-ph]].
- [13] S. Chakraborty, S. Choubey and K. Kar, “On the Observability of Collective Flavor Oscillations in Diffuse Supernova Neutrino Background,” *Phys. Lett. B* **702** (2011) 209 [arXiv:1006.3756 [hep-ph]].
- [14] S. Chakraborty, S. Choubey, B. Dasgupta and K. Kar, “Effect of Collective Flavor Oscillations on the Diffuse Supernova Neutrino Background,” *JCAP* **0809** (2008) 013 [arXiv:0805.3131 [hep-ph]].
- [15] F. P. An *et al.* [DAYA-BAY Collaboration], “Observation of electron-antineutrino disappearance at Daya Bay,” *Phys. Rev. Lett.* **108** (2012) 171803 [arXiv:1203.1669 [hep-ex]].
- [16] J. K. Ahn *et al.* [RENO Collaboration], “Observation of Reactor Electron Antineutrino Disappearance in the RENO Experiment,” *Phys. Rev. Lett.* **108**, 191802 (2012) [arXiv:1204.0626 [hep-ex]].
- [17] J. Gava and C. Volpe, “Collective neutrinos oscillation in matter and CP-violation,” *Phys. Rev. D* **78** (2008) 083007 [arXiv:0807.3418 [astro-ph]].
- [18] S. P. Mikheev and A. Yu. Smirnov, “Resonance amplification of oscillations in matter and spectroscopy of solar neutrinos,” *Yad. Fiz.* **42**, (1985) 1441 [*Sov. J. Nucl. Phys.* **42** (1985) 913].
- [19] L. Wolfenstein, “Neutrino Oscillations in Matter,” *Phys. Rev. D* **17** (1978) 2369.
- [20] H. Duan, G. M. Fuller and Y.-Z. Qian, “Collective Neutrino Oscillations,” *Ann. Rev. Nucl. Part. Sci.* **60** (2010) 569 [arXiv:1001.2799 [hep-ph]].
- [21] B. Dasgupta, E. P. O’Connor and C. D. Ott, “The Role of Collective Neutrino Flavor Oscillations in Core-Collapse Supernova Shock Revival,” *Phys. Rev. D* **85** (2012) 065008 [arXiv:1106.1167 [astro-ph.SR]].
- [22] A. Mirizzi and P. D. Serpico, “Instability in the dense supernova neutrino gas with flavor-dependent angular distributions,” *Phys. Rev. Lett.* **108** (2012) 231102 [arXiv:1110.0022 [hep-ph]].
- [23] N. Saviano, S. Chakraborty, T. Fischer and A. Mirizzi, “Stability analysis of collective neutrino oscillations in the supernova accretion phase with realistic energy and angle distributions,” arXiv:1203.1484 [hep-ph].
- [24] S. Chakraborty, T. Fischer, A. Mirizzi, N. Saviano and R. Tomàs, “Analysis of matter

- suppression in collective neutrino oscillations during the supernova accretion phase,” *Phys. Rev. D* **84** (2011) 025002 [arXiv:1105.1130 [hep-ph]].
- [25] S. Chakraborty, T. Fischer, A. Mirizzi, N. Saviano and R. Tomàs, “No collective neutrino flavor conversions during the supernova accretion phase,” *Phys. Rev. Lett.* **107** (2011) 151101 [arXiv:1104.4031 [hep-ph]].
- [26] S. Sarikas, G. G. Raffelt, L. Hüdepohl and H.-T. Janka, “Suppression of Self-Induced Flavor Conversion in the Supernova Accretion Phase,” *Phys. Rev. Lett.* **108** (2012) 061101 [arXiv:1109.3601 [astro-ph.SR]].
- [27] B. Dasgupta, A. Dighe, G. G. Raffelt and A. Yu. Smirnov, “Multiple Spectral Splits of Supernova Neutrinos,” *Phys. Rev. Lett.* **103** (2009) 051105 [arXiv:0904.3542 [hep-ph]].
- [28] G. Fogli, E. Lisi, A. Marrone and I. Tamborra, “Supernova neutrinos and antineutrinos: Ternary luminosity diagram and spectral split patterns,” *JCAP* **0910** (2009) 002 [arXiv:0907.5115 [hep-ph]].
- [29] B. Müller, H.-T. Janka and A. Marek, “A New Multi-Dimensional General Relativistic Neutrino Hydrodynamics Code for Core-Collapse Supernovae II. Relativistic Explosion Models of Core-Collapse Supernovae,” arXiv:1202.0815 [astro-ph.SR].
- [30] T. Fischer, S. C. Whitehouse, A. Mezzacappa, F.-K. Thielemann and M. Liebendörfer, “Protoneutron star evolution and the neutrino driven wind in general relativistic neutrino radiation hydrodynamics simulations,” *Astron. Astrophys.* **517** (2010) A80 [arXiv:0908.1871 [astro-ph.HE]].
- [31] C. Lunardini, “Diffuse neutrino flux from failed supernovae,” *Phys. Rev. Lett.* **102** (2009) 231101 [arXiv:0901.0568 [astro-ph.SR]].
- [32] K. Bays *et al.* [Super-Kamiokande Collaboration], “Supernova Relic Neutrino Search at Super-Kamiokande,” *Phys. Rev. D* **85** (2012) 052007 [arXiv:1111.5031 [hep-ex]].
- [33] M. Ikeda *et al.* [Super-Kamiokande Collaboration], *Astrophys. J.* **669** (2007) 519 [arXiv:0706.2283 [astro-ph]].
- [34] H. Yuksel and J. F. Beacom, “Neutrino Spectrum from SN 1987A and from Cosmic Supernovae,” *Phys. Rev. D* **76** (2007) 083007 [astro-ph/0702613 [ASTRO-PH]].
- [35] D. B. Cline, F. Raffaelli and F. Sergiampietri, “LANND: A line of liquid argon TPC detectors scalable in mass from 200 Tons to 100 Ktons,” *JINST* **1** (2006) T09001 [astro-ph/0604548].
- [36] A. Ereditato and A. Rubbia, “Conceptual design of a scalable multi-kton superconducting magnetized liquid Argon TPC,” *Nucl. Phys. Proc. Suppl.* **155** (2006) 233 [hep-ph/0510131].
- [37] A. Rubbia, “Underground Neutrino Detectors for Particle and Astroparticle Science: The Giant Liquid Argon Charge Imaging Experiment (GLACIER),” *J. Phys. Conf. Ser.* **171** (2009) 012020 [arXiv:0908.1286 [hep-ph]].
- [38] M. Wurm *et al.* [LENA Collaboration], “The next-generation liquid-scintillator neutrino observatory LENA,” *Astropart. Phys.* **35** (2012) 685 [arXiv:1104.5620 [astro-ph.IM]].
- [39] E. E. Salpeter, “The Luminosity function and stellar evolution,” *Astrophys. J.* **121** (1955) 161.
- [40] A. M. Hopkins and J. F. Beacom, “On the normalisation of the cosmic star formation history,” *Astrophys. J.* **651** (2006) 142 [astro-ph/0601463].
- [41] A. M. Hopkins, “The Star Formation History of the Universe,” [astro-ph/0611283].
- [42] W. Li, R. Chornock, J. Leaman, A. V. Filippenko, D. Poznanski, X. Wang, M. Ganeshalingam and F. Mannucci, “Nearby Supernova Rates from the Lick Observatory Supernova Search. III. The Rate-Size Relation, and the Rates as a Function of Galaxy Hubble Type and Colour,” arXiv:1006.4613 [astro-ph.SR].

- [43] L. E. Strigari, J. F. Beacom, T. P. Walker and P. Zhang, “The Concordance Cosmic Star Formation Rate: Implications from and for the supernova neutrino and gamma ray backgrounds,” *JCAP* **0504** (2005) 017 [astro-ph/0502150].
- [44] H. Shen, H. Toki, K. Oyamatsu and K. Sumiyoshi, “Relativistic equation of state of nuclear matter for supernova explosion,” *Prog. Theor. Phys.* **100** (1998) 1013 [nucl-th/9806095].
- [45] L. Hüdepohl, B. Müller, H.-T. Janka, A. Marek and G. G. Raffelt, “Neutrino Signal of Electron-Capture Supernovae from Core Collapse to Cooling,” *Phys. Rev. Lett.* **104** (2010) 251101 [Erratum-ibid. **105** (2010) 249901] [arXiv:0912.0260 [astro-ph.SR]].
- [46] B. Müller, A. Marek, H.-T. Janka and H. Dimmelmeier, “General Relativistic Explosion Models of Core-Collapse Supernovae,” arXiv:1112.1920 [astro-ph.SR].
- [47] M. T. Keil, G. G. Raffelt and H.-T. Janka, “Monte Carlo study of supernova neutrino spectra formation,” *Astrophys. J.* **590** (2003) 971 [astro-ph/0208035].
- [48] T. Fischer, private communication.
- [49] G. L. Fogli, E. Lisi, A. Marrone, A. Palazzo and A. M. Rotunno, “Evidence of $\theta_{13} > 0$ from global neutrino data analysis,” *Phys. Rev. D* **84** (2011) 053007 [arXiv:1106.6028 [hep-ph]].
- [50] G. L. Fogli, E. Lisi, A. Marrone, D. Montanino, A. Palazzo and A. M. Rotunno, “Global analysis of neutrino masses, mixings and phases: entering the era of leptonic CP violation searches,” arXiv:1205.5254 [hep-ph].
- [51] G. Sigl and G. G. Raffelt, “General kinetic description of relativistic mixed neutrinos,” *Nucl. Phys. B* **406** (1993) 423.
- [52] H. Duan, G. M. Fuller, J. Carlson and Y.-Z. Qian, “Simulation of Coherent Non-Linear Neutrino Flavor Transformation in the Supernova Environment. 1. Correlated Neutrino Trajectories,” *Phys. Rev. D* **74** (2006) 105014 [astro-ph/0606616].
- [53] B. Dasgupta and A. Dighe, “Collective three-flavor oscillations of supernova neutrinos,” *Phys. Rev. D* **77** (2008) 113002 [arXiv:0712.3798 [hep-ph]].
- [54] A. Friedland, “Self-refraction of supernova neutrinos: mixed spectra and three-flavor instabilities,” *Phys. Rev. Lett.* **104** (2010) 191102 [arXiv:1001.0996 [hep-ph]].
- [55] B. Dasgupta, A. Mirizzi, I. Tamborra and R. Tomàs, “Neutrino mass hierarchy and three-flavor spectral splits of supernova neutrinos,” *Phys. Rev. D* **81** (2010) 093008 [arXiv:1002.2943 [hep-ph]].
- [56] B. Dasgupta, G. G. Raffelt and I. Tamborra, “Triggering collective oscillations by three-flavor effects,” *Phys. Rev. D* **81** (2010) 073004 [arXiv:1001.5396 [hep-ph]].
- [57] A. S. Dighe and A. Yu. Smirnov, “Identifying the neutrino mass spectrum from the neutrino burst from a supernova,” *Phys. Rev. D* **62** (2000) 033007 [hep-ph/9907423].
- [58] G. L. Fogli, E. Lisi, A. Marrone and A. Mirizzi, “Collective neutrino flavor transitions in supernovae and the role of trajectory averaging,” *JCAP* **0712** (2007) 010 [arXiv:0707.1998 [hep-ph]].
- [59] A. Banerjee, A. Dighe and G. G. Raffelt, “Linearized flavor-stability analysis of dense neutrino streams,” *Phys. Rev. D* **84** (2011) 053013 [arXiv:1107.2308 [hep-ph]].
- [60] A. Esteban-Pretel, S. Pastor, R. Tomàs, G. G. Raffelt and G. Sigl, “Decoherence in supernova neutrino transformations suppressed by deleptonization,” *Phys. Rev. D* **76** (2007) 125018 [arXiv:0706.2498 [astro-ph]].
- [61] A. Esteban-Pretel, A. Mirizzi, S. Pastor, R. Tomàs, G. G. Raffelt, P. D. Serpico and G. Sigl, “Role of dense matter in collective supernova neutrino transformations,” *Phys. Rev. D* **78** (2008) 085012 [arXiv:0807.0659 [astro-ph]].

- [62] A. Mirizzi and R. Tomàs, “Multi-angle effects in self-induced oscillations for different supernova neutrino fluxes,” *Phys. Rev. D* **84** (2011) 033013 [arXiv:1012.1339 [hep-ph]].
- [63] C. Lunardini, B. Müller and H.-T. Janka, “Neutrino oscillation signatures of oxygen-neon-magnesium supernovae,” *Phys. Rev. D* **78** (2008) 023016 [arXiv:0712.3000 [astro-ph]].
- [64] J. F. Cherry, J. Carlson, A. Friedland, G. M. Fuller and A. Vlasenko, “Neutrino scattering and flavor transformation in supernovae,” arXiv:1203.1607 [hep-ph].
- [65] S. Sarikas, I. Tamborra, G. G. Raffelt, L. Hüdepohl and H.-T. Janka, “Supernova neutrino halo and the suppression of self-induced flavor conversion,” arXiv:1204.0971 [hep-ph].
- [66] J. M. Lattimer and M. Prakash, “Neutron star structure and the equation of state,” *Astrophys. J.* **550** (2001) 426 [astro-ph/0002232].